THE JOURNAL OF PHYSICAL CHEMISTRY B
A JOURNAL OF THE AMERICAN CHEMICAL SOCIETY

pubs.acs.org/JPCB Article

Facet Selectivity of Cetyltrimethyl Ammonium Bromide Surfactants on Gold Nanoparticles Studied Using Molecular Simulations

Abolfazl Faeli Qadikolae and Sumit Sharma*

Cite This: https://doi.org/10.1021/acs.jpcb.2c06236 Read Online

ACCESS | Metrics & More | Article Recommendations | Supporting Information

ABSTRACT: We have studied facet selectivity of cetyltrimethyl ammonium bromide (CTAB) surfactants of varying alkyl tail lengths (C_{17}TAB and C_{10}TAB) during their adsorption on a spherical gold metal nanoparticle (MNP) using umbrella sampling and well-tempered metadynamics techniques in molecular simulations. We show that the surfactants strongly adsorb with their alkyl tails wrapped around the MNP. The adsorption morphologies are dictated by the strong preference of the polar head group of the surfactants to adsorb on to the atoms that lie between the facets of the MNP, that is, in the vicinity of low-coordinated gold atoms. The alkyl tails do not display any strong facet preference. Owing to the longer alkyl tails, C_{17}TAB molecules pack together better than the C_{10}TAB molecules in the adsorbed state on the MNP. These findings suggest that the regions near the edges of the facets and low-coordinated atoms are expected to be preferentially covered with the adsorbed surfactants.

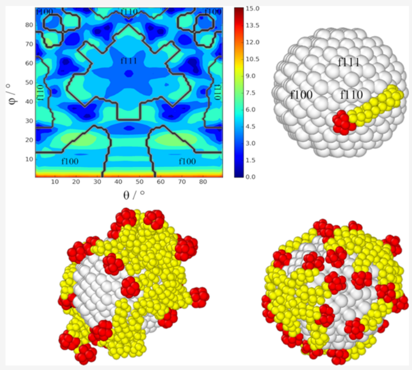

■ INTRODUCTION

Metallic nanoparticles (MNPs) have found important applications in bioimaging,[1] drug delivery,[2] molecular sensing,[3] nanofabrication,[4] and heterogeneous catalysis.[5] In many of these applications, the usefulness of MNPs arises from their distinct electrical, thermal, and optical properties. These properties are attributed to the collective oscillations of the conduction band electrons of MNPs in response to external electromagnetic fields, a phenomenon referred to as localized surface plasmon resonance. The nature of this resonance is a function of MNPs' size and shape.[6−9] MNPs also display unique catalytic properties, attributed to the high fractions of low-coordinated atoms on their surfaces.[10,11] Therefore, the ability to precisely control the size and shape of MNPs during their synthesis has garnered interest. A common approach for synthesizing MNPs is the seed-mediated growth method.[12−15] In this method, a faceted metallic crystal seed is first nucleated and then grown through the reduction of metal ions in solution via a reducing agent.[12,13] During the growth process, anisotropy in the shape of MNPs is imparted via the addition of surfactants, such as cetyltrimethylammonium bromide (CTAB).[12,13] It is presumed that this anisotropy is due to the preferential adsorption of surfactants on certain facets of the MNPs.[16] The adsorbed layer of surfactants creates a diffusion barrier for the metal ions on these facets, thereby retarding the growth.[16] In this synthesis process, the size and anisotropy of the MNPs are influenced by numerous factors, including surfactant concentration,[16] the alkyl tail length,[17] size of the polar group,[18] and type of counterions.[19] Previous experiments and molecular simulations have shown that longer alkyl tails, because of strong hydrophobic interactions, attain an organized packing of adsorbed surfactants on metal surfaces.[20,21] The role of hydrophobic interactions is also manifested in the morphologies attained by adsorbed surfactants as a function of size of the polar group. Surfactants with bulky polar groups adsorb as (hemi) spherical/cylindrical micelles, whereas the ones with small polar groups adsorb in a planar morphology.[22,23] Theoretical frameworks put forth to relate the types of surfactant morphologies to the molecular, solution, and interfacial characteristics have achieved varying degrees of success.[22,24−27] Previous studies that have examined facet selectivity during the adsorption have implicated factors including the differential arrangement of water close to the metal facets,[28,29] changes in counterion concentration near the facets during the adsorption,[30] different adsorbed morphologies and packing densities of the surfactants,[31,32] and role of additives in modulating interfacial free energies of the facets.[33] Clearly, there are multiple factors at play and a comprehensive picture of the phenomenon has remained elusive.

In this work, we have studied adsorption of CTAB surfactants [Figure 1] on a faceted spherical gold MNP via molecular dynamics simulation. We find that these surfactants have a strong tendency to adsorb on to the MNP and they adsorb by wrapping around the MNP surface. The adsorption morphology is dictated by the preference of the polar head of

Received: August 31, 2022
Revised: October 26, 2022

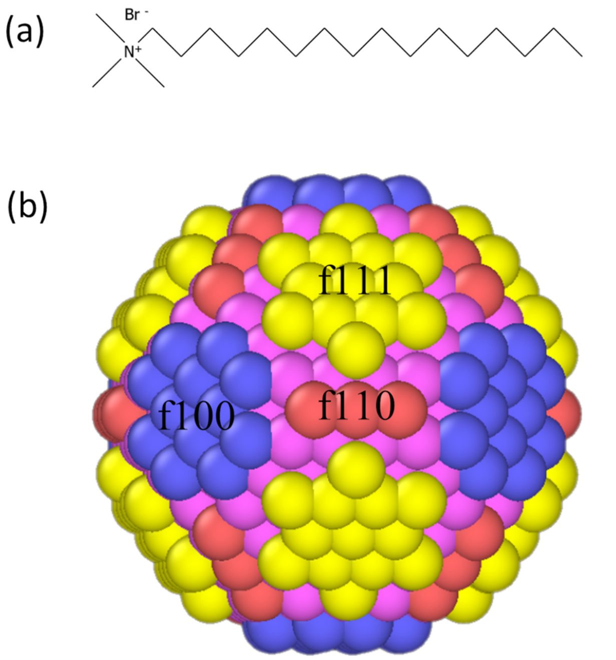

Figure 1. (a) Cetyltrimethylammonium bromide (CTAB), (b) The faceted rigid gold metal nanoparticle (MNP) of diameter 30 Å employed in this study.

the surfactants for regions in between the facets. These regions harbor low-coordinated gold atoms. Furthermore, upon comparing the adsorption behavior of C_{17}TAB and C_{10}TAB (that is, CTAB surfactants with a 17 carbon and 10 carbon long alkyl tail, respectively), we find that hydrophobic interactions between the longer alkyl tails cause C_{17}TAB to adsorb in a more aggregated morphology. Our results provide important insights into the factors that govern the facet selectivity during the adsorption of CTAB surfactants on MNPs.

■ SIMULATION SYSTEM AND METHODS

Our simulation system comprises of a gold nanoparticle, one or more surfactant molecules, and water molecules. The gold nanoparticle, henceforth referred to as MNP, studied by us is a face-centered cubic arrangement of gold atoms forming a faceted sphere of around 30 Å diameter [Figure 1(b)]. The MNP has (111), (110), and (100) facets and in between these facets are some surface-exposed atoms, which we term as "iAu". It is well understood that gold nanoparticles of size of 5 nm and less have high fractions of low-coordinated corner/edge atoms.[34−36] Gold atoms in a close-packed surface have nine neighbors, which decreases to seven on steps on the surface, and to three or four at the corners.[37] Density functional theory (DFT) studies[38] and classical Monte Carlo simulations[39] show that in the case of small nanoparticles (∼5 nm and less), the crystallographic structures may depart from those predicted by the Wulff construction to harbor low-coordinated atoms on their surfaces. Furthermore, in the synthesis of surfactant-mediated anisotropic gold nanoparticles, it is hypothesized that the first step involves the formation of spherical gold seeds of size ∼3 to 5 nm, after which symmetry breaking in the structure occurs, which results in the formation of different well-defined facets.[40] One would expect the spherical gold seeds to have low-coordinated atoms prior to symmetry breaking. We have simulated our constructed gold nanoparticle in water (without surfactants) for 5 ns in the canonical ensemble at 300 K while keeping the gold atoms mobile. In this simulation, the MNP retains its structure except for the restructuring of one low-coordinated surface atom [Figure S1b, Supporting Information]. The "iAu" atoms, that is, the atoms between the facets, remain exposed to the solvent after the 5 ns simulation run. Water is modeled using the single point charge enhanced (SPC/E) model.[41] For the infinite dilution simulations, the system comprises of 20,000 water molecules. For the simulations with 30 surfactant molecules, we have 25,000 water molecules. We have studied the adsorption behavior of C_{10}TAB and C_{17}TAB molecules. Interactions of gold atoms are modeled via the interface force field developed by the Heinz group.[42] Gold atoms are charge-neutral. Charges on the surfactant molecules are calculated by performing B3LYP-level DFT with 6-31G(d,p) basis sets in implicit water solvent. The interactions of surfactants are modeled via the General Amber Force Field (GAFF).[43] Bromide ion parameters are taken from the Joung−Cheatham model.[44] We use PACKMOL to generate the initial configurations.[45] Coulombic interactions are calculated via Particle−Particle−Particle Mesh (PPPM) Ewald. A spherical cutoff of 10 Å is chosen for Lennard-Jones as well as the real space part of Coulombic interactions. Isothermal−Isobaric (NPT) simulations (temperature T = 300 K and pressure P = 1 bar) using the Nose-Hoover thermostat and barostat are performed with 1 femtosecond (fs) timestep. Periodic boundary conditions (PBC) are applied in all the three directions. The MNP is treated as a rigid body fixed in space. All simulations are performed using the Large-scale Atomic/Molecular Massively Parallel Simulator (LAMMPS) software.[46]

Adsorption Free Energy Calculations. We calculate the adsorption free energy of a surfactant molecule on the MNP in infinite dilution using umbrella sampling.[47] Umbrella sampling is performed by choosing the radial distance of the center of mass of the surfactant from the center of the MNP as the order parameter. The biasing potential is thus given by $U(\xi, \xi_i) = \frac{1}{2}K(\xi - \xi_i)^2$, where K is the force constant, ξ is the set value of the center of mass distance for an umbrella sampling window, and ξ_i is the center of mass distance of the surfactant from the center of the MNP in a configuration. The value of K is chosen to ensure that the adjacent umbrella sampling windows have sufficient overlap. For $\xi_i > 22$ Å, we set $K = 5$ kcal/mol/Å^2. For $\xi_i < 22$ Å, we vary the K from 10 to 100 kcal/mol/Å^2 to ensure that all the radial distances are adequately sampled. A large value of the K needed at smaller distances as the surfactant has a strong affinity for the MNP. Each umbrella sampling window is run for 50 ns for equilibration followed by 10 ns of production run, and the error bars are generated from three independent simulations. The umbrella sampling biasing potential is removed via the weighted histogram method (WHAM) to obtain the adsorption free energy profiles as a function of ξ.[48]

Well-Tempered Metadynamics. We use well-tempered metadynamics to study the preferential adsorption of the polar head group of the surfactant molecules on the MNP.[49] The rationale for studying the adsorption preference of the polar group is that in our MD simulations, we observe the polar group to distinctly prefer to adsorb on to the atoms in between the facets (termed as the iAu atoms). The alkyl tails do not exhibit such a preference. In the well-tempered metadynamics simulation, the order parameter is the location of the polar

https://doi.org/10.1021/acs.jpcb.2c06236
J. Phys. Chem. B XXXX, XXX, XXX−XXX

group on the MNP surface, defined by the θ and φ angles in the spherical coordinates with the center of the MNP as the origin. A repulsive barrier is placed at a distance of 6 Å from the MNP surface to prevent the polar group from diffusing away from the MNP. In metadynamics, a history-dependent bias potential, in the form of Gaussian functions, is added to allow efficient sampling of the phase space.[49] The total bias potential added during the course of metadynamics is stored in a grid in the collective variable space for efficient evaluation of the overall bias potential. For our simulation, we select the grid size of 1.5° and width of the Gaussian potential to be 3°. In well-tempered metadynamics, height of the Gaussian bias potentials is decreased based on the extent of sampling of the phase space region.[49] The rate at which the height is decreased is controlled by a bias factor. In our simulation, the bias factor is set to 8 and the initial Gaussian height to 0.1 kcal/mol. The Gaussian potentials are added after every 1000 steps. The simulation is performed for 600 ns. We implement both umbrella sampling and well-tempered metadynamics using the COLVARS package in LAMMPS.[50]

■ RESULTS AND DISCUSSION

First, we have calculated the adsorption free energy of $C_{10}TAB$ and $C_{17}TAB$ on the spherical gold MNP in infinite dilution using the umbrella sampling methodology. Figure 2 shows the free energy profiles as a function of the radial distance between the center of mass of the surfactants and the center of the MNP, ξ. Both $C_{10}TAB$ and $C_{17}TAB$ adsorb strongly on the MNP with no free energy barrier. Figure 2 also shows snapshots of the $C_{17}TAB$ system at different distances from the MNP. The free energy profiles display a shoulder that is associated with an ensemble of configurations wherein the polar group of the surfactants adsorbs on to the MNP and the alkyl tail remains dangling in the solution (see the snapshot in Figure 2). Because the applied biasing potential is a function of the radial distance, diffusion of the surfactant molecule around the MNP is not restricted. It is noteworthy to mention that the polar group always ends up adsorbing on the iAu atoms (that is, the atoms in between the facets) of the MNP. At the free energy minimum, the surfactant molecule is wrapped around the MNP as shown. The adsorption free energies of $C_{10}TAB$ and $C_{17}TAB$ are found to be 10.04 ± 0.03 and 12.57 ± 0.37 kcal/mol, respectively. In comparison, the adsorption free energies of $C_{10}TAB$ and $C_{16}TAB$ on the flat gold (111) surface were found to be around 21.5 and 22.5 kcal/mol, respectively.[51] The significantly lower adsorption free energy on the MNP in comparison to the flat surface is due to the unfavorable free energy associated with the bending configurations that the adsorbed molecules attain on the MNP.

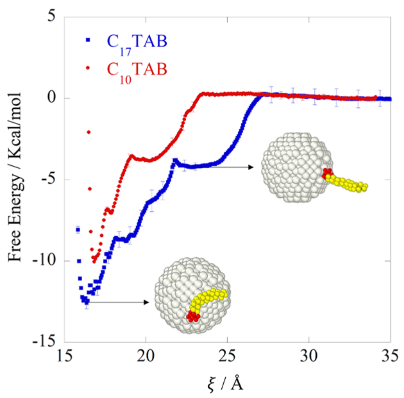

Figure 2. Free energy profiles of $C_{10}TAB$ and $C_{17}TAB$ molecules as a function of distance between the center of mass of the surfactant and the center of the MNP, ξ. Error bars are standard deviation calculated from three independent simulations.

We find in our umbrella sampling simulations that the polar group prefers to adsorb on to the iAu atoms. To further validate this observation, we perform well-tempered metadynamics to study the free energy landscape of the adsorbed polar group on the MNP surface as a function of its location. The order parameter in this case is the (θ, φ) angles in spherical coordinates that identifies the location of the polar group on the MNP surface. Figure 3 shows the free energy landscape that is obtained after 600 ns of the well-tempered metadynamics simulation. Figure S2 (Supporting Information) shows that the error in the free energy landscape is not more than 0.8 kcal/mol. It is observed that the minima in the free energy coincide with the location of the iAu atoms on the MNP surface, which clearly highlights the preference of the polar group for the iAu atoms. Another interesting observation seen for f111 and f100 facets is that the free energy of adsorption on these facets is favorable near the center of the facets rather than close to their edge [Figure 3]. We have also calculated the average binding energy of the polar group on the different facets [Figure 4]. The binding energy is most favorable for the iAu atoms and is similar in magnitude for the f111 and f100 facets. The f110 facet comprises of only three atoms and thus is not a complete facet [see Figure 1(b)]. Therefore, it is concluded that the adsorption preference of the polar group on the iAu atoms is dominated by its favorable binding energy.

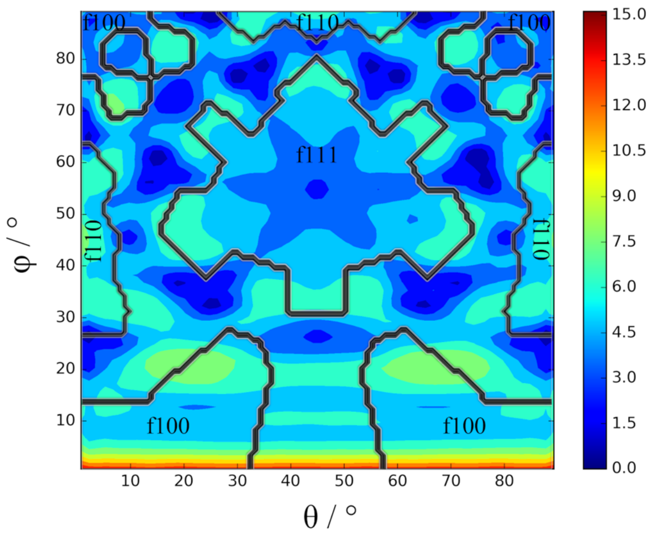

Figure 3. Free energy landscape of the adsorbed polar group on the MNP as a function of θ and φ angles in spherical coordinates with the center of the MNP as the origin. Color scale is in the units of kcal/mol. This landscape is generated via a well-tempered metadynamics simulation.

Now that we understand the adsorption behavior of a single surfactant molecule, it is interesting to study how multiple surfactant molecules adsorb on to the MNP. For this study, we perform six independent isothermal−isobaric ensemble (NPT) MD simulations of 30 $C_{17}TAB$ molecules in the presence of the MNP. Snapshots of the initial configurations of these

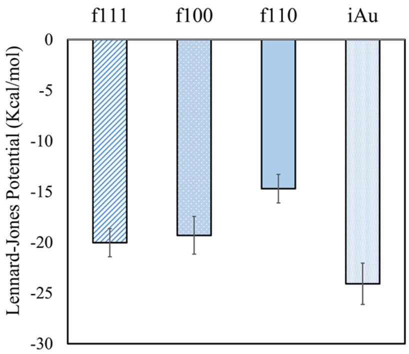

Figure 4. Average binding energy of the polar group with the different facets of the MNP. Error bars are standard deviation from 1000 different configurations of the polar group adsorbed on each facet.

simulations are shown in Figure S3 (Supporting Information). The simulations are equilibrated for 200 ns followed by a production run of 40 ns. Figure 5a shows the location where the polar group of the surfactant molecules adsorb on the MNP. For this calculation, we determine the number of polar groups that adsorb on a facet normalized by the number of atoms that comprise the facet. We observe that the polar groups preferentially adsorb on the iAu atoms, similar to the behavior of a single surfactant molecule. Their adsorption preference is similar for the f111 and f100 facets. The error bars in Figure 5a are obtained as the standard deviation of the adsorption amount in the six simulations. Interestingly, because the iAu atoms are preferred by the polar group, alkyl tails end up not adsorbing on the iAu but adsorb on the f111, f110, and f100 facets [Figure S4 (Supporting Information)]. For C_{10}TAB, we perform three independent NPT ensemble simulations of 30 molecules near the MNP. Figure 5b shows the location where the polar groups of the C_{10}TAB adsorb on the MNP. A similar trend as Figure 5a is observed, that is, the polar groups adsorb preferentially on the iAu atoms.

Figure 6 shows snapshots of the adsorbed configurations of C_{17}TAB and C_{10}TAB molecules on the MNP. In the C_{17}TAB system, 22 ± 4 molecules adsorb on the MNP, whereas in the C_{10}TAB system, 28.6 ± 0.5 molecules adsorb. The MNP surface coverage is 72.0 ± 6.3% and 78.0 ± 0.2% for the C_{17}TAB and C_{10}TAB systems, respectively. While in infinite dilution, the free energy of adsorption of C_{17}TAB is 2 kcal/mol lower than that of C_{10}TAB, a greater number of C_{10}TAB molecules adsorb in these simulations. C_{17}TAB molecules also

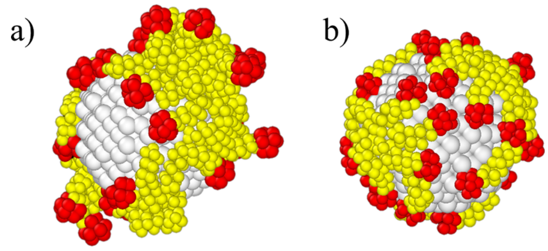

Figure 6. Snapshots showing the adsorbed configurations of (a) C_{17}TAB and (b) C_{10}TAB when 30 surfactant molecules are introduced in the simulation box. C_{17}TAB forms a more aggregated configuration as compared to C_{10}TAB. Polar groups in both the systems preferentially adsorb on to the iAu atoms.

show a larger fluctuation in the number of adsorbed molecules. One reason for this observation could be that C_{17}TAB prefer to adsorb in a more aggregated morphology, which limits the number of adsorbed molecules if they cannot be accommodated in the aggregated state. Indeed, we observe that in the adsorbed configuration, the alkyl tails of C_{17}TAB molecules prefer to align parallel to each other to maximize their interactions. To quantify the aggregation of the alkyl tails, we compute the coordination number of the methylene/methyl groups given by $C(z) = \sum_{i=1}^{N} \frac{1-\left(\frac{Z_i-3}{Z_0}\right)^6}{1-\left(\frac{Z_i-3}{Z_0}\right)^{12}}$, where Z_i is the distance between the carbon atoms of different molecules. We set the point of inflection, Z_0 = 5 Å. Figure 7 compares the

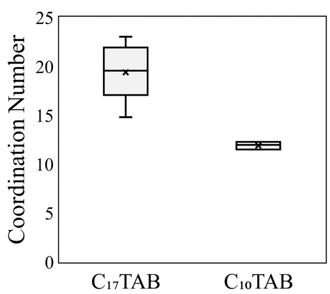

Figure 7. Box and whisker plot of the coordination number of the alkyl tails of adsorbed surfactant molecules. Alkyl tails of C_{17}TAB aggregates strongly in the adsorbed state because of the favorable hydrophobic interactions between them.

$C(z)$ for the adsorbed C_{17}TAB and C_{10}TAB tails in a box and whisker plot. The $C(z)$ of C_{17}TAB is much higher than that of

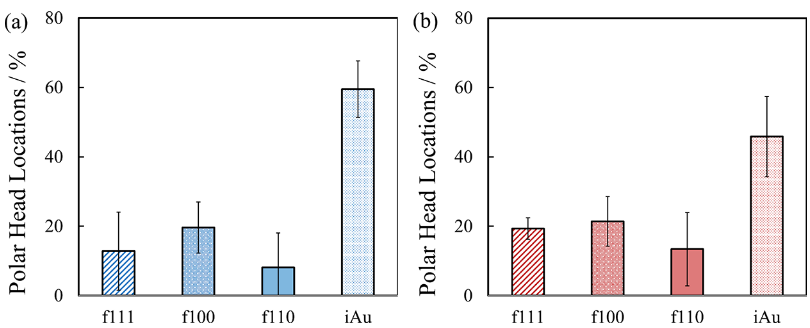

Figure 5. Adsorption location of polar groups of (a) C_{17}TAB and (b) C_{10}TAB surfactants on the MNP for simulations comprising 30 surfactant molecules with the MNP. Number of polar groups adsorbed on a facet is normalized by the number of atoms that comprise the facet. Error bars are standard deviation calculated from six and three independent simulations for C_{17}TAB and C_{10}TAB, respectively.

https://doi.org/10.1021/acs.jpcb.2c06236
J. Phys. Chem. B XXXX, XXX, XXX−XXX

$C_{10}TAB$, which confirms that the alkyl tails of $C_{17}TAB$ aggregate more in the adsorbed configuration, which is in accordance with the experimental results.[20] The distribution profiles of the polar group of the surfactants as a function of their distance from the MNP [Figure S5 (Supporting Information)] show a single peak, implying that both $C_{17}TAB$ and $C_{10}TAB$ surfactants adsorb as a single layer on the MNP in our simulations.

In our previous work, we have reported that a large free energy barrier is associated with the adsorption of $C_{10}TAB$ and $C_{17}TAB$ micelles on a flat gold surface because of which the micelles do not adsorb on the surfaces within the simulation time scales.[52] We acknowledge that at, present, we have not done an extensive investigation of the behavior of surfactant micelles close to the MNP. However, in a canonical ensemble simulation of $C_{17}TAB$ micelles close to the MNP, we observe that the micelle adsorbs onto the MNP within a ns [Figure S6, Supporting Information]. Then, in the next 40 ns, the micelle completely disintegrates, and the constituent surfactant molecules adsorb onto the MNP. From this preliminary study, it is likely that there is no free energy barrier to micelle adsorption on the MNP, which may be due to the small size of the MNP that does not perturb the spherically symmetric solvation shell of the micelle. However, this assertion requires a more detailed study. A difference between this study and the previous one on micelle adsorption on flat metal surfaces is that in this study, we have bromides as counterions, while in the previous case, the counterions were chlorides.

CONCLUSIONS

We have studied adsorption behavior of $C_{17}TAB$ and $C_{10}TAB$ molecules on a faceted spherical gold MNP. We find that both the surfactant molecules have strong affinity to adsorb on the MNP with no free energy barrier in infinite dilution. The molecules adsorb by wrapping themselves around the MNP. Our main conclusion is that the polar groups of the CTAB molecules show a strong preference to adsorb onto the iAu atoms on the surface, that is, the atoms in between two facets of the MNP. The strong preference for iAu is due to the stronger binding energy that the polar group has for the iAu atoms as compared to the facets. In the adsorption studies of a large number of surfactant molecules, it is observed that the adsorption morphology is dictated by the polar groups preferring to adsorb on the iAu atoms. The alkyl tails end up adsorbing on the f111, f100, and f110 facets of the MNP. Because of the longer alkyl tails, in the adsorption of $C_{17}TAB$ molecules, the alkyl tails prefer to aggregate with each other. Overall, these results provide important insights into the facet selectivity of surfactant adsorption, which forms the basis of surfactant-mediated synthesis of anisotropic MNPs, as well as has implications for applications, such as in heterogeneous catalysis.[5] Previous studies have shown that MNPs have unique catalytic properties because of the presence of a high fraction of low-coordinated atoms on their surfaces.[34−36] Our study corroborates these findings by showing that the surfactant molecules indeed demonstrate a preference for adsorption at these low-coordinated atoms. The presence of surfactants or impurities in the system may render these atoms inactive through adsorption during catalytic reactions and thus alter the reaction yield. In surfactant-mediated synthesis of MNPs, preferential adsorption of surfactants in between the facets may play a role in imparting anisotropy by hindering the lateral growth of the facets. It will be interesting to study how the adsorption morphology changes as more surfactants adsorb onto the MNP. In our study, the size of the polar head group is larger than the iAu region. A smaller polar group may manifest an even stronger preference for adsorption on the iAu atoms.

ASSOCIATED CONTENT

Supporting Information

The Supporting Information is available free of charge at https://pubs.acs.org/doi/10.1021/acs.jpcb.2c06236.

Faceted gold nanoparticles with the different facets; difference between the free energy profiles in the last 30 ns of the metadynamics simulation; initial configurations used for studying adsorption of 30 $C_{17}TAB$ molecules on MNP; adsorption preferences of the alkyl tails of the surfactants for different facets of the MNP; distribution profile of the polar groups of the surfactants as a function of their distance from the center of the MNP; and snapshots showing the adsorption and disintegration of a $C_{17}TAB$ micelle near the MNP (PDF)

AUTHOR INFORMATION

Corresponding Author

Sumit Sharma − *Department of Chemical and Biomolecular Engineering, Ohio University, Athens, Ohio 45701, United States*; orcid.org/0000-0003-3138-5487; Email: sharmas@ohio.edu

Author

Abolfazl Faeli Qadikolae − *Department of Chemical and Biomolecular Engineering, Ohio University, Athens, Ohio 45701, United States*; orcid.org/0000-0002-6555-8895

Complete contact information is available at: https://pubs.acs.org/10.1021/acs.jpcb.2c06236

Notes

The authors declare no competing financial interest.

ACKNOWLEDGMENTS

This work is supported by the National Science Foundation (NSF) CAREER grant 2046095. Computational resources for this work were provided by Ohio Supercomputer Center (project number PAA0031) and National Science Foundation XSEDE grant number DMR190005.

REFERENCES

(1) Bardhan, R.; Lal, S.; Joshi, A.; Halas, N. J. Theranostic Nanoshells: From Probe Design to Imaging and Treatment of Cancer. *Acc. Chem. Res.* **2011**, *44*, 936−946.

(2) Horiguchi, Y.; Niidome, T.; Yamada, S.; Nakashima, N.; Niidome, Y. Expression of Plasmid DNA Released from DNA Conjugates of Gold Nanorods. *Chem. Lett.* **2007**, *36*, 952−953.

(3) Nusz, G. J.; Marinakos, S. M.; Curry, A. C.; Dahlin, A.; Hök, F.; Wax, A.; Chilkoti, A. Label-Free Plasmonic Detection of Biomolecular Binding by a Single Gold Nanorod. *Anal. Chem.* **2008**, *80*, 984−989.

(4) Wang, Y.; DePrince, A. E.; Gray, S. K.; Lin, X.-M.; Pelton, M. Solvent-Mediated End-to-End Assembly of Gold Nanorods. *J. Phys. Chem. Lett.* **2010**, *1*, 2692−2698.

(5) Marshall, S. T.; O'Brien, M.; Oetter, B.; Corpuz, A.; Richards, R. M.; Schwartz, D. K.; Medlin, J. W. Controlled Selectivity for Palladium Catalysts Using Self-Assembled Monolayers. *Nat. Mater.* **2010**, *9*, 853−858.

(6) Jain, P. K.; Lee, K. S.; El-Sayed, I. H.; El-Sayed, M. A. Calculated Absorption and Scattering Properties of Gold Nanoparticles of

Different Size, Shape, and Composition: Applications in Biological Imaging and Biomedicine. *J. Phys. Chem. B* **2006**, *110*, 7238−7248.

(7) Sau, T. K.; Rogach, A. L.; Jäckel, F.; Klar, T. A.; Feldmann, J. Properties and Applications of Colloidal Nonspherical Noble Metal Nanoparticles. *Adv. Mater.* **2010**, *22*, 1805−1825.

(8) Zhan, W.; Shu, Y.; Sheng, Y.; Zhu, H.; Guo, Y.; Wang, L.; Guo, Y.; Zhang, J.; Lu, G.; Dai, S. Surfactant-Assisted Stabilization of Au Colloids on Solids for Heterogeneous Catalysis. *Angew. Chem., Int. Ed.* **2017**, *56*, 4494−4498.

(9) Seo, J.; Lee, S.; Koo, B.; Jung, W. Controlling the Size of Pt Nanoparticles with a Cationic Surfactant, CnTABr. *CrystEngComm* **2018**, *20*, 2010−2015.

(10) Abad, A.; Concepción, P.; Corma, A.; García, H. A Collaborative Effect between Gold and a Support Induces the Selective Oxidation of Alcohols. *Angew. Chem., Int. Ed.* **2005**, *44*, 4066−4069.

(11) Hughes, M. D.; Xu, Y.-J.; Jenkins, P.; McMorn, P.; Landon, P.; Enache, D. I.; Carley, A. F.; Attard, G. A.; Hutchings, G. J.; King, F.; Stitt, E. H.; Johnston, P.; Griffin, K.; Kiely, C. J. Tunable Gold Catalysts for Selective Hydrocarbon Oxidation under Mild Conditions. *Nature* **2005**, *437*, 1132−1135.

(12) Jana, N. R.; Gearheart, L.; Murphy, C. J. Wet Chemical Synthesis of High Aspect Ratio Cylindrical Gold Nanorods. *J. Phys. Chem. B* **2001**, *105*, 4065−4067.

(13) Nikoobakht, B.; El-Sayed, M. A. Preparation and Growth Mechanism of Gold Nanorods (NRs) Using Seed-Mediated Growth Method. *Chem. Mater.* **2003**, *15*, 1957−1962.

(14) Jana, N.; Wang, Z.; Sau, T.; Pal, T. Seed-Mediated Growth Method to Prepare Cubic Copper Nanoparticles. *Curr. Sci.* **2000**, *79*, 1367.

(15) Niu, W.; Zhang, L.; Xu, G. Seed-Mediated Growth of Noble Metal Nanocrystals: Crystal Growth and Shape Control. *Nanoscale* **2013**, *5*, 3172−3181.

(16) Murphy, C. J.; Sau, T. K.; Gole, A. M.; Orendorff, C. J.; Gao, J.; Gou, L.; Hunyadi, S. E.; Li, T. Anisotropic Metal Nanoparticles: Synthesis, Assembly, and Optical Applications. *J. Phys. Chem. B* **2005**, *109*, 13857−13870.

(17) Gao, J.; Bender, C. M.; Murphy, C. J. Dependence of the Gold Nanorod Aspect Ratio on the Nature of the Directing Surfactant in Aqueous Solution. *Langmuir* **2003**, *19*, 9065−9070.

(18) Kou, X.; Zhang, S.; Tsung, C.-K.; Yeung, M. H.; Shi, Q.; Stucky, G. D.; Sun, L.; Wang, J.; Yan, C. Growth of Gold Nanorods and Bipyramids Using CTEAB Surfactant. *J. Phys. Chem. B* **2006**, *110*, 16377−16383.

(19) Kawasaki, H.; Nishimura, K.; Arakawa, R. Influence of the Counterions of Cetyltrimetylammonium Salts on the Surfactant Adsorption onto Gold Surfaces and the Formation of Gold Nanoparticles. *J. Phys. Chem. C* **2007**, *111*, 2683−2690.

(20) Khan, M. R.; Singh, H.; Sharma, S.; Asetre Cimatu, K. L. Direct Observation of Adsorption Morphologies of Cationic Surfactants at the Gold Metal−Liquid Interface. *J. Phys. Chem. Lett.* **2020**, *11*, 9901−9906.

(21) Singh, H.; Sharma, S. Determination of Equilibrium Adsorbed Morphologies of Surfactants at Metal-Water Interfaces Using a Modified Umbrella Sampling-Based Methodology. *J. Chem. Theory Comput.* **2022**, *18*, 2513−2520.

(22) Ko, X.; Sharma, S. A Quantitatively Accurate Theory to Predict Adsorbed Configurations of Asymmetric Surfactant Molecules on Polar Surfaces. *J. Phys. Chem. B* **2020**, *124*, 5517−5524.

(23) Ko, X.; Sharma, S. Adsorption and Self-Assembly of Surfactants on Metal−Water Interfaces. *J. Phys. Chem. B* **2017**, *121*, 10364−10370.

(24) Nagarajan, R.; Ruckenstein, E. Theory of Surfactant Self-Assembly: A Predictive Molecular Thermodynamic Approach. *Langmuir* **1991**, *7*, 2934−2969.

(25) Johnson, R. A.; Nagarajan, R. Modeling Self-Assembly of Surfactants at Solid/Liquid Interfaces. I. Hydrophobic Surfaces. *Colloids Surf., A* **2000**, *167*, 31−46.

(26) Johnson, R. A.; Nagarajan, R. Modeling Self-Assembly of Surfactants at Solid−Liquid Interfaces. II. Hydrophilic Surfaces. *Colloids Surf., A* **2000**, *167*, 21−30.

(27) Sharma, S.; Singh, H.; Ko, X. A Quantitatively Accurate Theory To Predict Adsorbed Configurations of Linear Surfactants on Polar Surfaces. *J. Phys. Chem. B* **2019**, *123*, 7464−7470.

(28) Ramezani-Dakhel, H.; Ruan, L.; Huang, Y.; Heinz, H. Molecular Mechanism of Specific Recognition of Cubic Pt Nanocrystals by Peptides and of the Concentration-Dependent Formation from Seed Crystals. *Adv. Funct. Mater.* **2015**, *25*, 1374−1384.

(29) Qi, X.; Jin, B.; Cai, B.; Yan, F.; De Yoreo, J.; Chen, C.-L.; Pfaendtner, J. Molecular Driving Force for Facet Selectivity of Sequence-Defined Amphiphilic Peptoids at Au−Water Interfaces. *J. Phys. Chem. B* **2022**, *126*, 5117−5126.

(30) da Silva, J. A.; Meneghetti, M. R. New Aspects of the Gold Nanorod Formation Mechanism via Seed-Mediated Methods Revealed by Molecular Dynamics Simulations. *Langmuir* **2018**, *34*, 366−375.

(31) Ruan, L.; Ramezani-Dakhel, H.; Chiu, C.-Y.; Zhu, E.; Li, Y.; Heinz, H.; Huang, Y. Tailoring Molecular Specificity Toward a Crystal Facet: A Lesson From Biorecognition Toward Pt{111}. *Nano Lett.* **2013**, *13*, 840−846.

(32) Meena, S. K.; Sulpizi, M. Understanding the Microscopic Origin of Gold Nanoparticle Anisotropic Growth from Molecular Dynamics Simulations. *Langmuir* **2013**, *29*, 14954−14961.

(33) Qi, X.; Fichthorn, K. A. Theory of the Thermodynamic Influence of Solution-Phase Additives in Shape-Controlled Nanocrystal Synthesis. *Nanoscale* **2017**, *9*, 15635−15642.

(34) Janssens, T. V. W.; Clausen, B. S.; Hvolbæk, B.; Falsig, H.; Christensen, C. H.; Bligaard, T.; Nørskov, J. K. Insights into the Reactivity of Supported Au Nanoparticles: Combining Theory and Experiments. *Top. Catal.* **2007**, *44*, 15.

(35) Burch, R. Gold Catalysts for Pure Hydrogen Production in the Water−Gas Shift Reaction: Activity, Structure and Reaction Mechanism. *Phys. Chem. Chem. Phys.* **2006**, *8*, 5483−5500.

(36) Lopez, N.; Janssens, T. V. W.; Clausen, B. S.; Xu, Y.; Mavrikakis, M.; Bligaard, T.; Nørskov, J. K. On the Origin of the Catalytic Activity of Gold Nanoparticles for Low-Temperature CO Oxidation. *J. Catal.* **2004**, *223*, 232−235.

(37) Hvolbæk, B.; Janssens, T. V. W.; Clausen, B. S.; Falsig, H.; Christensen, C. H.; Nørskov, J. K. Catalytic Activity of Au Nanoparticles. *Nano Today* **2007**, *2*, 14−18.

(38) McKenna, K. P.; Shluger, A. L. Shaping the Morphology of Gold Nanoparticles by CO Adsorption. *J. Phys. Chem. C* **2007**, *111*, 18848−18852.

(39) Brodersen, S. H.; Grønbjerg, U.; Hvolbæk, B.; Schiøtz, J. Understanding the Catalytic Activity of Gold Nanoparticles through Multi-Scale Simulations. *J. Catal.* **2011**, *284*, 34−41.

(40) Lohse, S. E.; Murphy, C. J. The Quest for Shape Control: A History of Gold Nanorod Synthesis. *Chem. Mater.* **2013**, *25*, 1250−1261.

(41) Berendsen, H. J. C.; Grigera, J. R.; Straatsma, T. P. The Missing Term in Effective Pair Potentials. *J. Phys. Chem.* **1987**, *91*, 6269−6271.

(42) Heinz, H.; Vaia, R. A.; Farmer, B. L.; Naik, R. R. Accurate Simulation of Surfaces and Interfaces of Face-Centered Cubic Metals Using 12−6 and 9−6 Lennard-Jones Potentials. *J. Phys. Chem. C* **2008**, *112*, 17281−17290.

(43) Wang, J.; Wolf, R. M.; Caldwell, J. W.; Kollman, P. A.; Case, D. A. Development and Testing of a General Amber Force Field. *J. Comput. Chem.* **2004**, *25*, 1157−1174.

(44) Joung, I. S.; Cheatham, T. E. Determination of Alkali and Halide Monovalent Ion Parameters for Use in Explicitly Solvated Biomolecular Simulations. *J. Phys. Chem. B* **2008**, *112*, 9020−9041.

(45) Martínez, L.; Andrade, R.; Birgin, E. G.; Martínez, J. M. PACKMOL: A package for building initial configurations for molecular dynamics simulations. *J. Comput. Chem.* **2009**, *30*, 2157−2164.

https://doi.org/10.1021/acs.jpcb.2c06236
J. Phys. Chem. B XXXX, XXX, XXX−XXX

(46) Plimpton, S. Fast Parallel Algorithms for Short-Range Molecular Dynamics. *J. Comput. Phys.* **1995**, *117*, 1−19.
(47) Torrie, G. M.; Valleau, J. P. Nonphysical Sampling Distributions in Monte Carlo Free-Energy Estimation: Umbrella Sampling. *J. Comput. Phys.* **1977**, *23*, 187−199.
(48) Souaille, M.; Roux, B. Extension to the Weighted Histogram Analysis Method: Combining Umbrella Sampling with Free Energy Calculations. *Comput. Phys. Commun.* **2001**, *135*, 40−57.
(49) Barducci, A.; Bussi, G.; Parrinello, M. Well-Tempered Metadynamics: A Smoothly Converging and Tunable Free-Energy Method. *Phys. Rev. Lett.* **2008**, *100*, No. 020603.
(50) Fiorin, G.; Klein, M. L.; Hénin, J. Using Collective Variables to Drive Molecular Dynamics Simulations. *Mol. Phys.* **2013**, *111*, 3345−3362.
(51) Singh, H.; Sharma, S. Free Energy Profiles of Adsorption of Surfactant Micelles at Metal-Water Interfaces. *Mol. Simul.* **2021**, *47*, 420−427.
(52) Singh, H.; Sharma, S. Disintegration of Surfactant Micelles at Metal−Water Interfaces Promotes Their Strong Adsorption. *J. Phys. Chem. B* **2020**, *124*, 2264.

https://doi.org/10.1021/acs.jpcb.2c06236
J. Phys. Chem. B XXXX, XXX, XXX−XXX